Journal of Institute of Science and Technology, 26(2), 127-136 (2021)
ISSN: 2467-9062 (print), e-ISSN: 2467-9240
https://doi.org/10.3126/jist.v26i2.41664

Research Article

BOX COUNTING FRACTAL DIMENSION AND FREQUENCY SIZE DISTRIBUTION OF EARTHQUAKES IN THE CENTRAL HIMALAYA REGION

Ram Krishna Tiwari[1,2,*] Harihar Paudyal[2]
[1]Central Department of Physics, Tribhuvan University, Kirtipur, Kathmandu
[2]Birendra Multiple Campus, Tribhuvan University, Bharatpur, Chitwan
**Corresponding author: E-mail: ram.tiwari@bimc.tu.edu.np*
(Received:** July 30, 2021; **Revised:** December 25, 2021; **Accepted:** December 28, 2021**)

ABSTRACT

To establish the relations between b-value and fractal dimension (D_0) for the earthquake distribution, we study the regional variations of those parameters in the central Himalaya region. The earthquake catalog of 989 events (Mc = 4.0) from 1994.01.31 to 2020.10.28 was analyzed in the study. The study region is divided into two sub-regions (I) Region A: 27.3°N -30.3°N and 80°E -84.8°E (western Nepal and vicinity) and (II) Region B: 26.4°N -28.6°N and 84.8°E -88.4°E (eastern Nepal and vicinity). The b-value observed is within the range between 0.92 to 1.02 for region A and 0.64 to 0.74 for region B showing the homogeneous nature of the variation. The seismic a-value for those regions ranges respectively between 5.385 to 6.007 and 4.565 to 5.218. The low b-values and low seismicity noted for region B may be related with less heterogeneity and high strength in the crust. The high seismicity with average b-values obtained for region A may be related with high heterogeneity and low strength in the crust. The fractal dimension ≥1.74 for region A and ≥ 1.82 for region B indicate that the earthquakes were distributed over two-dimensional embedding space. The observed correlation between D_0 and b is negative for western Nepal and positive for eastern Nepal while the correlation between D_0 and a/b value is just opposite for the respective regions. The findings identify both regions as high-stress regions. The results coming from the study agree with the results of the preceding works and reveal information about the local disparity of stress and change in tectonic complexity in the central Himalaya region.

Keywords: b-value, complexity, fractal dimension, central Himalaya, stress

INTRODUCTION

On 25 April of 2015, the central Nepal was struck by Mw 7.8 (6.9 mb) earthquake. The event took place on the Main Himalayan Thrust (MHT) (Adhikari *et al.*, 2015; Yue *et al.*, 2017) and was resulted from unfastening of the lower edge of the sealed portion of the MHT, along which the Himalayan hunk is thrust over India (Avouac *et al.*, 2015). The MHT is the dynamic structure along the Himalayan arc and reaches the surface at Main Frontal Thrust (MFT) as observed by the Japanese Agency (Hubbard *et al.*, 2015). Within the 17 days (on 12 May 2015), the nation was again struck by another earthquake of Mw 7.3 (6.7 mb) (Lindsey *et al.*, 2015). These two large events with their aftershocks have partly released the strain accumulated between seismic events along the MHT (Hayes *et al.*, 2015; Sreejith *et al.*, 2018). The mainshock and prompt running aftershock sequence caused strong ground shaking not only in Nepal but also in some parts of neighboring nations India and China, causing more than 8900 deaths (Lindsey *et al.*, 2015). Ground shaking in Kathmandu basin was strong enough to collapse many historical structures that had persisted the preceding earthquakes(Galetzka *et al.*, 2015).

From the study of literatures, the spreading of the rupture in the past Himalayan earthquakes were understood to be organized by asperities and supplementary structural complexities (Bilham, 2019; Mugnier *et al.*, 2017). Since the Gorkha earthquake of 2015 happened between the rupture areas of the 1505 Ms 8.2 Lo-Mustang earthquake in western Nepal (Ghazoui *et al.*, 2019) and Nepal-Bihar earthquake (Mw 8.2) of 1934, it was expected to have the magnitude greater than 8 (Letort *et al.*, 2016). Sreejith *et al.* (2018) disclose the existence high strain and stress region (asperity), one towards the west and the other towards the east of the 2015 Gorkha epicenter. Although, the asperity found in the eastern side had broken partially in the Gorkha earthquake, the asperity in the western side is still unbroken and preparing to host the future large earthquake. Furthermore, it is known that the elastic potential energy releasing process in the Himalaya is either by the large rupture reaching the surfaces or by incomplete rupture (Scholz & Campos, 2012). The case of partial rupture for Gorkha earthquake indicates the event did not release all the stored strain in the region and the region is overdue for major earthquake (Avouac *et al.*, 2015; Ghazoui *et al.*, 2019). This investigation applies the theory of nonlinear dynamics (Helmstetter *et al.*, 2005; Yin *et al.*, 2019) to identify the stress regions in terms of b-values and box counting fractal dimension of epicenter distribution. Based on the previous studies on the aftermath of the Gorkha earthquake, the study region is divided into two sub-regions (Fig. 1).

(I) Region A: 27.3°N - 30.3°N and 80°E - 84.8°E (western Nepal and vicinity) consisting of 348 earthquakes.
(II) Region B: 26.4°N - 28.6°N and 84.8°E - 88.4°E (eastern Nepal and vicinity) consisting of 274 earthquakes.

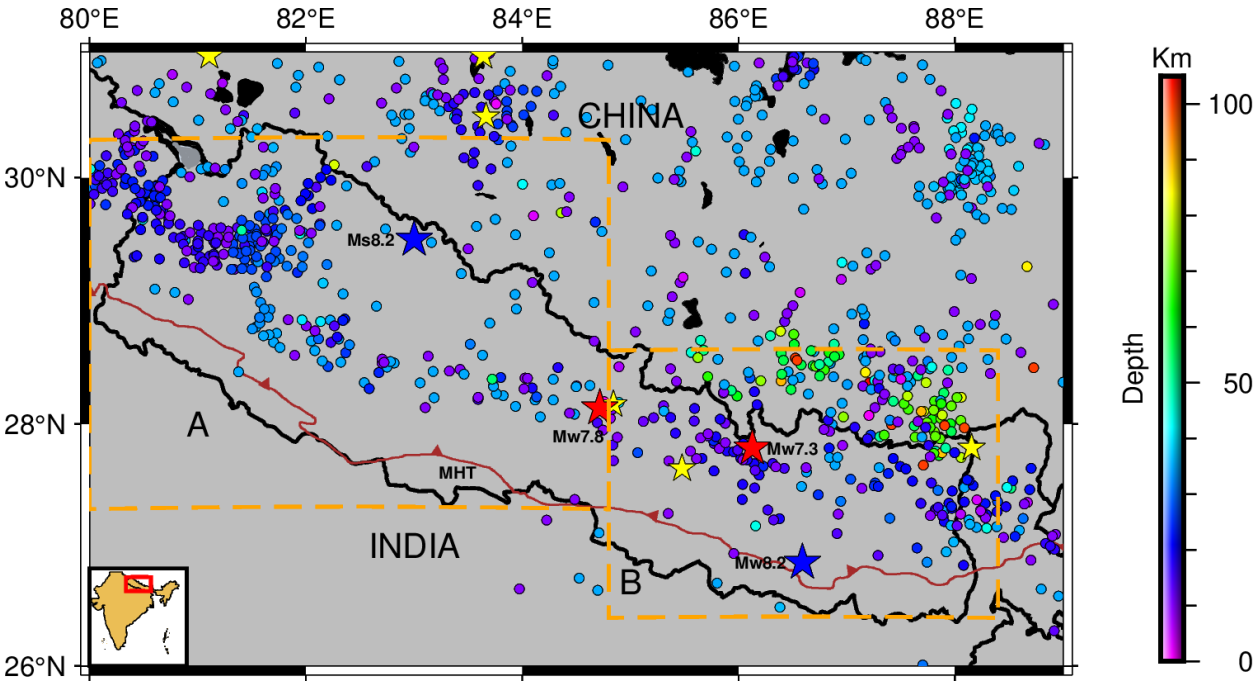

Figure 1. Epicentral locations of the 1189 earthquakes events out of which 1181 events with magnitude ≤ 5.9 mb are represented by solid circle. The color of the circle indicates the depth of the earthquake events. Yellow stars stand for the 6 earthquake events ≥ 6 mb after 1994 and two red stars stand for Mw 7.8 Gorkha earthquake and Mw 7.3 Dolakha earthquake. Blue star in the region A stands for 1505 Lo-Mustang earthquake (Ms 8.2) and blue star in the region B stands for 1934 Nepal-Bihar earthquake (Mw 8.2). Regions of interest are demarcated by orange box into regions A and B. Inset map at bottom left corner of the map shows study region bounded by red box.

Data

The earthquake events were collected from International Seismological Centre (ISC) catalog and United States Geological Survey (USGS) catalog. While selecting the events priority was given to ISC catalog and events were scrutinized on the basis of locations (latitude and longitude) and date with time of occurrence The Mw scale of USGS catalog were converted into mb scale from the relation given by Das *et al.* (2011). We found 2457 events for the period 1964-02-01 to 2020-11-23 with in the latitude 26°N to 31°N and longitude 80°E to 89°E. After declustering the catalog (Gardner & Knopoff, 1974) from the software ZMAP (Wiemer, 2001) , we only retained 1185 events. The software ZMAP is the widely accepted tool for the statistical analysis of the seismicity pattern so equally applicable for the study in the Himalayan region. The cumulative curve (Fig. 2) shows straight line with constant slope after January 1994 giving the completeness (Mc=4.0) of catalog, so the catalog starts from 1994 with 989 events. For the analysis of the epicenters, we have selected rectangular areas of dimension 3°×3° in the region A (sub-regions A1 to A10) and 3°×2.2° in the region B (sub-regions B1to B4) as mentioned in the Table 1 and Table 2. The variation between b and D_0 over time was evaluated using sliding windows of aforementioned areas with window advance of 0.2 degree along the direction of longitude in order to cover region of the study. The time number histograms (Fig. 3) display the high seismic activity in region A compared to region B whereas the increase of seismic activity around the year 2015 is observed for both regions.

METHODOLOGY

Earthquake frequency size distribution b-value

The cumulative frequency size dispersal of earthquakes is given by the relation.

$$Log\ N_c = a - bM$$

where N_c is the number of earthquakes with magnitude greater or equal to M, a is the constant signifying the level of the productivity and b is the constant known as b-value that signifies magnitude distribution (Gutenberg & Richter, 1944). The frequency-magnitude analysis of the data is done by the maximum curvature technique and the b-value is estimated by maximum likelihood approach (Aki, 1965).

$$\mathrm{b} = \frac{\log_{10} e}{M_{av.} - (M - \Delta M/2)}$$

where $M_{av.}$ is the average value of the magnitudes, M is the lower limit of the magnitude in the catalog and ΔM is the binning width of the catalog. The uncertainty occurred in the estimation of the b-value is given by the relation below (Shi & Bolt, 1982).

$$\delta \mathrm{b} = 2.3 * \mathrm{b}^2 \sqrt{\frac{\sum_i^N (M_i - M_{av.})^2}{n_c(n_c - 1)}}$$

where n_c is the number of earthquakes in the given sample. The magnitude of completeness (Mc) was determined as 4.0 (for 989 events) using the iterative method (Wiemer & Wyss, 2000). The b-value is normally inferred as the sign of the heterogeneity present in the material of the medium and found to fluctuate from 1.0 to 1.6 for the global seismicity (Mogi, 1967; Sobiesiak *et al.*, 2007). Also, it is interpreted as the indicator of applied tangential stresses (Scholz, 1968; Schorlemmer *et al.*, 2005; Singh *et al.*, 2009). For the earthquakes in the California, the b-values found to vary from 0.45 to 1.5 (Gutenberg & Richter, 1944). The b-value of 0.80 ± 0.05 is computed for aftershocks sequences of Gorkha earthquake between 2015 May 25 and June 8 (Adhikari *et al.*, 2015). For the 820 aftershocks (2.7 < M < 7.3) of the Gorkha earthquake, the b-value of 1.11 ± 0.08 was computed during the period April 25 – November 12, 2015 (Nampally *et al.*, 2018). The b-values for the longitude range 80°E to 89°E and latitude range 26°N to 31°N found to vary from 0.5 to 1.6 for the period 1964-2015 (Ghosh, 2020). Furthermore, the b-value contour map depicts the low b-value patch in the western part of the Gorkha region as the possible zone of future robust seismic activity (Tiwari & Paudyal, 2021).

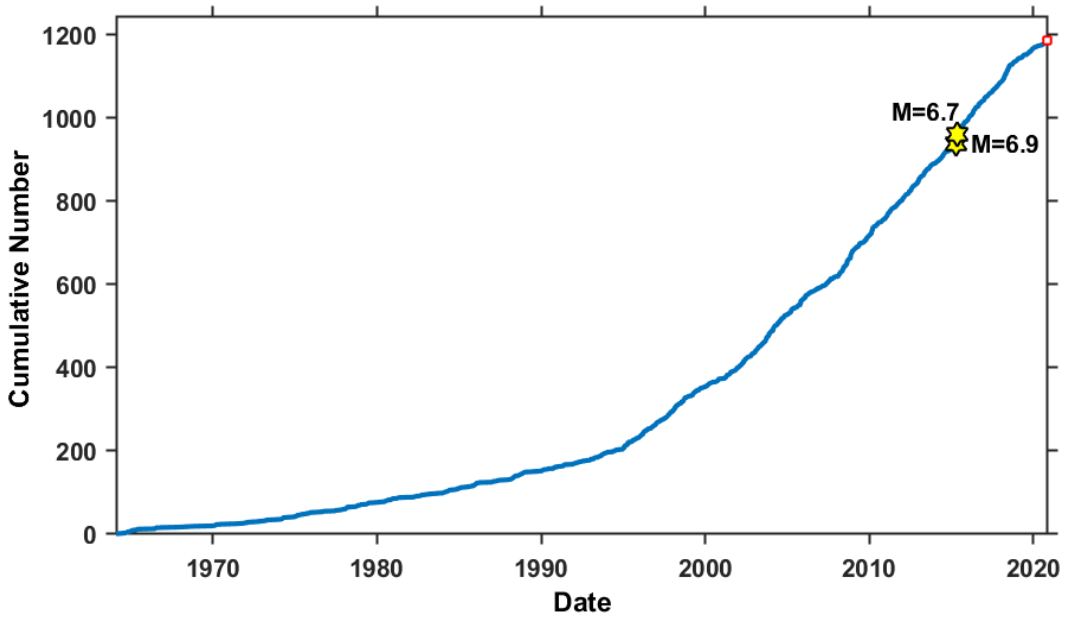

Figure 2. Cumulative number of events with time showing 6.9 mb Gorkha earthquake and 6.7 mb major aftershock

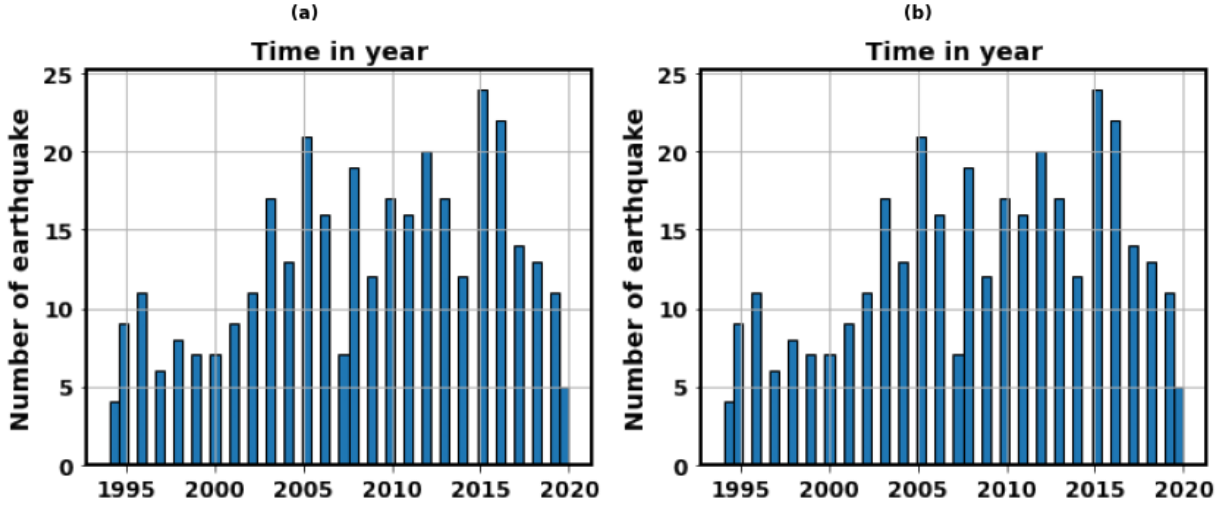

Figure 3. Time histograms of the earthquakes for (a) region A and (b) region B

Fractal distribution

A distribution with fracture or uneven basic structure reiterate in different scales is a fractal. The index providing a statistical value to compare how a pattern alters with the measuring scale is the fractal dimension (Lopes & Betrouni, 2009). Earthquakes are known as self-organized dynamical

system progressing spatially and temporarily towards a critical stationary stage, so the fractal theories are beneficial in learning seismic activities (Rodríguez Pascua *et al.*, 2003). The spectrum of the fractal dimension can be obtained from the generalized fractal dimension D_q and it is calculated from the relation (Grassberger & Procaccia, 1983).

$$C_q\ (N_c, r) = [\frac{1}{N_c}\sum_{i=1}^{N_c}[\frac{1}{N_c - 1}\sum_{j=1, i\neq j}^{N}\theta\big(r - \|X_i - X_j\|\big)]^{q-1}]^{\frac{1}{q-1}}$$

In above equation, $\theta\big(r - \|X_i - X_j\|\big) = \begin{cases} 1, if\ \|X_i - X_j\| < r \\ 0, if\ \|X_i - X_j\| \geq r \end{cases}$ is the Heaviside step function, r is the scaling radius, N_c is the total number of pair of data points within the sample volume, X_i and X_j are the location of the epicenter in latitude and longitude of the i^{th} event and the j^{th} event while $C_q\ (N_c, r)$ is the q^{th} integral.

The generalized dimension D_q, in terms of generalized correlation sum can be written as,

$$D_q = \lim_{r\to 0}\frac{1}{q-1}\frac{\log C_q(N_c, r)}{\log r}$$

For the monofractal having homogeneous epicentral distribution, D_q has the constant values for all q values (Zamani & Agh-Atabai, 2011).

Moreover, $\lim_{N_c\to\infty} C_q(N_c, r) = C_q(r)$

Finally, the generalized dimension$\big(D_q\big)$, in terms of the generalized correlation sum

$$D_q = \lim_{r\to 0}\frac{1}{q-1}\frac{\log C_q(r)}{\log r}$$

For q = 0, the above formula gives capacity dimension. It gives information dimension for q=1, and correlation dimension for q=2 (Roy & Padhi, 2007). Therefore, for q = 0, the formula reduces to

$$D_0 = -\lim_{r\to 0}\frac{\log C_q(r)}{\log r}$$

The above formula is similar to the box counting technique (Aggarwal *et al.*, 2017; Mandal & Rodkin, 2011; Radziminovich *et al.*, 2019) as

$$D_0 = -\lim_{r\to 0}\frac{\log N_c(r)}{\log r}$$

where N_c(r) is the number of boxes of side r occupied by point sources. With the advantage of simple mathematical formulation and empirical estimation, box-counting dimension becomes the widely used dimension (Falconer, 1997). The box counting technique estimates the capacity dimension by measuring the space-filling characters of a fracture set with the change in grid of the scale (Gospodinov *et al.*, 2010; Mandal & Rodkin, 2011). In the box-counting method, the epicenter distribution is covered by squares or cubes of decreasing size (r). If the epicenter distribution points have fractal character the slope of the $\log C_q(r) - \log r$ curve, in particular range of r, provides capacity dimension.

RESULTS AND DISCUSSION

The b-value of the region A ranges from 0.91 ± 0.08 to1.02 ± 0.10 (Table 1; Fig. 4a) while b-value of Region B ranges from 0.64 ± 0.04 to 0.78 ± 0.06 (Table 2; Fig. 5a). The relatively high b-value and high seismicity observed in the region A may indicate that the area is linked with high material heterogeneity and low strength in the crust as explained in the literatures Mogi (1967) and Scholz (1968). Many small earthquakes can be expected in regions. The low b-values and relatively low seismicity in the region B may be linked with low degree of heterogeneity and strong rheological strength in the crust that approves the preceding works (Bayrak *et al.*, 2013; Khan *et al.*, 2011; Khattri & Tyagi, 1983; Wyss, 1973). The creeping process occurring in the faults is generally related with higher b-value, and asperities present in the faults are often related to lower b-value (Kawamura & Chen, 2017; Oncel & Wilson, 2002). Thus, the earthquakes in the region A may be due to the creeping process and the dominating number of aftershock in the region B are related to the asperities found in the region.

The fractal dimension of the region A ranges from 1.79 ± 0.01 to 1.89 ± 0.03 (Table 1; Fig. 4b). Similarly, for the region B it ranges from 1.82 ± 0.02 to 1.86 ± 0.02 (Table 2; Fig. 5b). These non-integers values of the dimension between 1 and 2 indicates that the earthquakes are spread on the boundary between a line and a plane (Rodríguez Pascua *et al.*, 2003). Tosi (1998) explained that possible values of fractal dimensions do not depend on the dimension of the embedding space and the value ranges between 0 and 2. The limiting value of dimension can be interpreted as D_0 close to 0 has all events bunched into single point, D_0 near to 1 means the source region has linear nature and D_0 near to 2 shows that the epicenters are casually or evenly spread over a two-dimensional (2D) implanting space (Roy & Ram, 2006; Tosi, 1998). Thus, the higher D_0 (1.79 -1.89) obtained for the regions may be the indication of scattered epicenter distributions. The lowest b-values and the highest D_0 computed for region B indicate the vulnerability of the region for occurrence of the large earthquakes (Naimi-Ghassabian *et al.*, 2018). The works similar to the present investigation have been carried out by the previous researchers. The fractal correlation dimension of 1.66 is noted for 820 aftershocks between April 25 – November 12, 2015 for Gorkha earthquake (Nampally et al., 2018). The fractal dimension of 1.69 ± 0.05 is obtained for the epicenter distribution of 2001 Bhuj earthquake (Mw 7.7) in Gujarat, India (Aggarwal et al., 2017).

Table 1. Subdivided regions of A with period, location, earthquakes numbers, frequency magnitude distribution coefficients a-value and b-value, ratio of a and b, fractal dimension (D_0) and coefficient of determination (R^2)

Region/period	Latitude/Longitude	No. of events	a-value	b-value	a/b	D_0	R^2
A1 (1994-01-31—2020-10-28)	27.3°N-30.3°N 80.0°E-83.0°E	277	5.817	0.92 ± 0.06	6.32	1.88 ± 0.03	0.993
A2 (1994-01-31—2020-10-28)	27.3°N-30.3°N 80.2°E-83.2°E	267	5.809	0.93 ± 0.06	6.24	1.87 ± 0.03	0.993
A3 (1994-01-31—2020-10-28)	27.3°N-30.3°N 80.4°E-83.4°E	250	5.763	0.92 ± 0.06	6.26	1.89 ± 0.03	0.994
A4 (1994-01-31—2020-10-28)	27.3°N-30.3°N 80.6°E-83.6°E	241	5.780	0.93 ± 0.07	6.21	1.88 ± 0.02	0.995
A5 (1994-01-31—2020-10-28)	27.3°N-30.3°N 80.8°E-83.8°E	228	5.894	0.97 ± 0.07	6.07	1.88 ± 0.02	0.994
A6 (1994-01-31—2020-03-15)	27.3°N-30.3°N 81.0°E-84.0°E	224	5.897	0.97 ± 0.07	6.08	1.86 ± 0.02	0.994
A7 (1994-01-31—2020-03-15)	27.3°N-30.3°N 81.2°E -84.2°E	210	5.995	1.00 ± 0.01	6.00	1.82 ± 0.03	0.993
A8 (1994-01-31—2020-03-15)	27.3°N-30.3°N 81.4°E -84.4°E	200	5.868	0.97 ± 0.01	6.04	1.79 ± 0.02	0.994
A9 (1994-01-31—2020-03-15)	27.3°N-30.3°N 81.6°E -84.6°E	168	5.979	1.02 ± 0.10	5.87	1.79 ± 0.01	0.999
A10 (1994-05-10—2020-03-15)	27.3°N-30.3°N 81.8°E -84.8°E	139	5.385	0.91 ± 0.08	5.92	1.74 ± 0.01	0.998
Entire A (1994-01-31—2020-10-28)	27.3°N-30.3°N 80.0°E -84.8°E	348	6.007	0.95 ± 0.06	6.32	1.87 ± 0.02	0.995

Table 2. Subdivided regions of B with period, location, earthquakes numbers, frequency magnitude distribution coefficients a-value and b-value, ratio of a and b, fractal dimension (D_0) and coefficient of determination (R^2)

Region/Period	Latitude/Longitude	No. of events	a-value	b-value	a/b	D_0	R^2
B1 (1994-06-25—2020-11-23)	26.4°N -28.6°N 84.8°E -87.8°E	202	4.565	0.64 ± 0.04	7.13	1.82 ± 0.02	0.997
B2 (1994-05-25—2020-11-23)	26.4°N -28.6°N 85.0°E -88.0°E	234	5.218	0.78 ± 0.06	6.69	1.82 ± 0.02	0.995
B3 (1994-05-25—2020-11-23)	26.4°N -28.6°N 85.2°E -88.2°E	250	5.211	0.78 ± 0.06	6.68	1.84 ± 0.02	0.996
B4 (1994-05-25—2020-11-23)	26.4°N -28.6°N 85.4°E -88.4°E	257	5.205	0.77 ± 0.05	6.76	1.85 ± 0.02	0.996
Entire B (1994-05-25—2020-11-23)	26.4°N -28.6°N 84.8°E -88.4°E	274	5.137	0.74 ± 0.05	6.94	1.86 ± 0.02	0.996

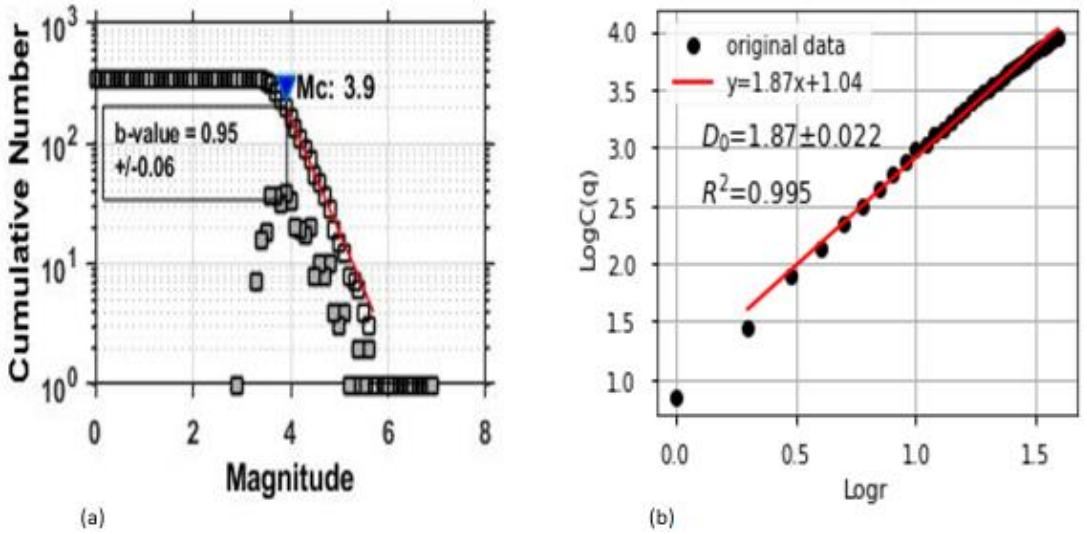

Figure 4. Graphs showing (a) Frequency magnitude distribution b-value and (b) D_0 for the entire region A.

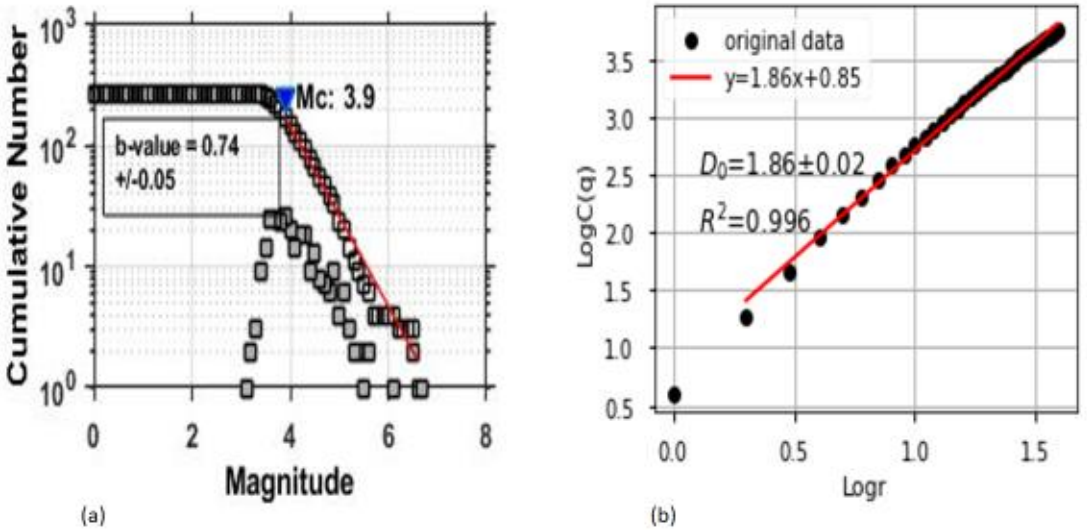

Figure 5. Graphs showing (a) Frequency magnitude distribution b-value and (b) D_0 for the entire region B

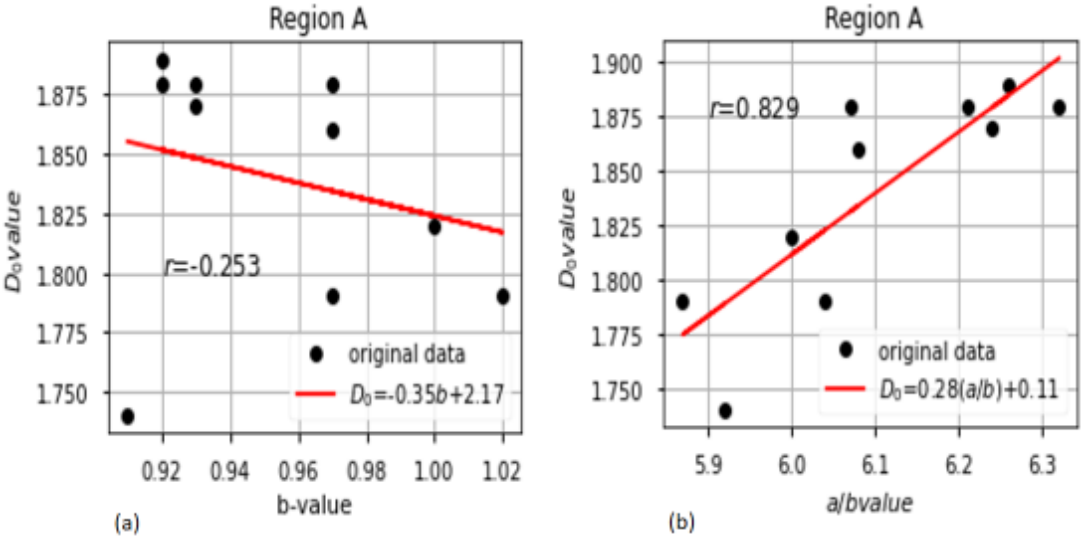

Figure 6. Correlation between variations in D_0 and (a) b-value and (b) the ratio $^{a}/_{b}$ for region A

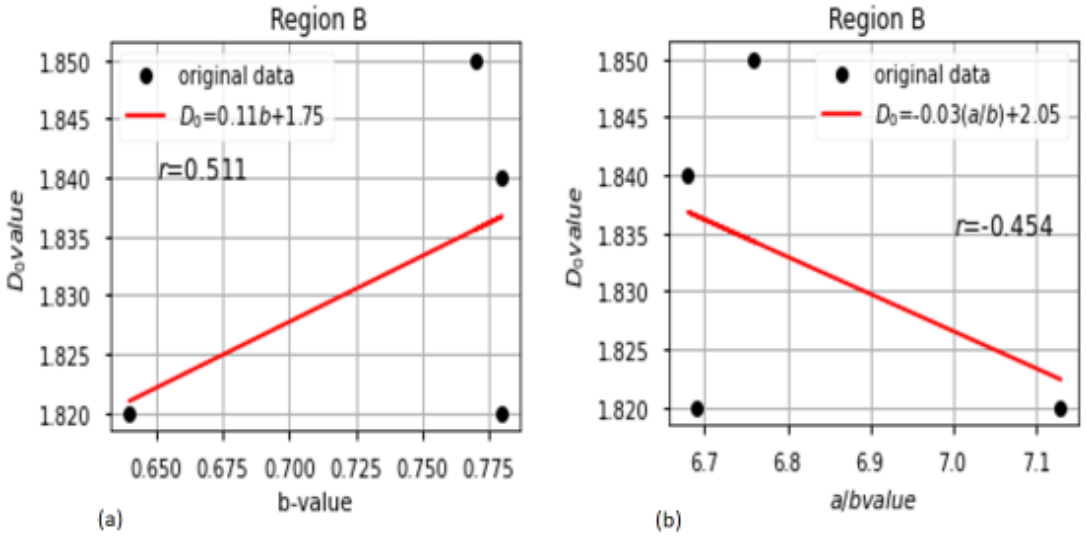

Figure 7. Correlation between variations in D_0 and (a) b-value and (b) the ratio $^{a}/_{b}$ for region B

The D_0 – b and D_0 – (a/b) relations could possibly replicate regional seismicity and earthquake threat and believed to be applicable in earthquake hazard related studies (Bayrak & Bayrak, 2012; Pailoplee & Choowong, 2014). The negative correlations between b-value and D_0 (r = - 0.253) is obtained for the region A (Fig. 6a) while the positive correlation (r = 0.511) is observed in the region B (Fig. 6b). The positive correlations between a/b and D_0 (r = 0.829) is observed for the region A (Fig. 6b) and negative correlation (r = - 0.454) is observed for the region B (Fig. 7b). The D_0 – (a/b) correlation was explained to be quite dependable and effective comparing to the D_0 – b correlation for indicating seismic hazards(Bayrak & Bayrak, 2012), but in this work, it is justified only for the region A showing the significant of the distribution of D_0 – a/b with r = 0.829. The negative correlations mean the drop in one parameter for rise in another and the positive correlations means parallel increase or decrease in corresponding parameters. The drop in D_0 and rise in b-value or parallel rise or fall in D_0 and a/b for the region A indicate the presence of dense and complex network of faults having likelihood of occurring earthquake with larger magnitude (Oncel & Wilson, 2007). The positive correlation between D_0 and b or negative correlation between D_0 and a/b in region B can be interpreted as reduced probability of larger magnitude earthquake because the stress in the region is reducing through lower magnitude events. The preceding study had also noticed negative correlation between b-value and fractal dimension for this region from the earthquake data of seismological catalogs of the USGS and ISC (Ghosh, 2020).

For the region A, there is a decrease in D_0 and increase in b-value as the sliding windows move from west to east while for the region B both parameters increase as the window moves from west to east (Fig. 8). Thus, the spatial variation of D_0 and b-value is in the negative correlation for the region A and in the positive correlation for the region B. The negative spatial correlation may be responsible to the rise in stress concentration (lower b) and a decline in the clustering of the epicenter (increased D_0).

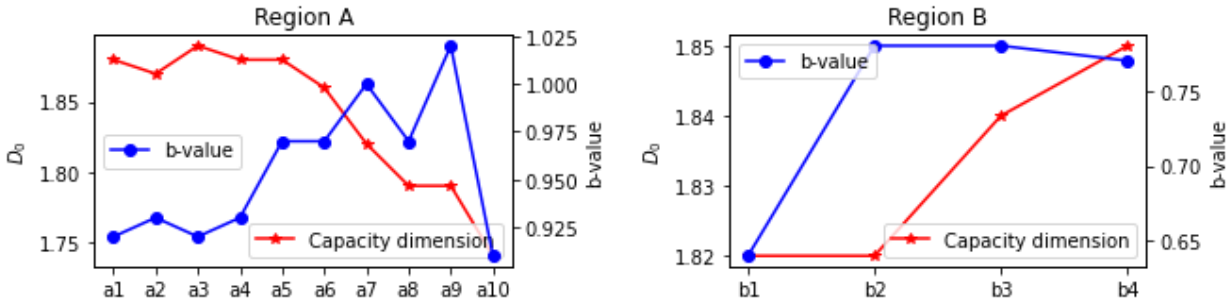

Figure 8. Regional variation of b-value and D_0 depending on the windows selected

CONCLUSIONS

The analysis is carried out on earthquake catalog (Mc = 4.0) of 989 events from January 1994 to November 2020. The spatial variation of fractal dimension (D_0) with b-value shows negative correlation for western Nepal and vicinity while correlation is positive for eastern Nepal and vicinity. The correlation of D_0 with a/b ratio is just opposite. From these results, it can be inferred that regions considered are under high stress and posing risk for generating large earthquake in the future. The western Nepal is safe against the seismic hazards as the b-value of the region is getting average b-value of 1.0 through the small earthquakes event. The observed low b values for eastern Nepal imply that it is highly stressed and could be a source region for future strong events. The high fractal dimension value ≥1.74 obtained for both regions indicate the earthquake events are distributed in two-dimensional embedding space (source zones). This study indicates the regional variation of stress level and difference in tectonic complexity.

ACKNOWLEDGEMENTS

The first author (Ram Krishna Tiwari) would like to acknowledge Tribhuvan University, Nepal, and University Grants Commission (UGC), Nepal for the sabbatical leave and financial support, respectively.

AUTHOR CONTRIBUTIONS

HP conceived and designed the research. RKT handled the software, analyzed and interpreted the data. Both authors wrote and revised the manuscript.

CONFLICT OF INTEREST

The authors declare no conflict of interest.

DATA AVAILABILITY STATEMENT

The data that support the findings of this study are available from the corresponding author, upon reasonable request.

REFERENCES

Adhikari, L.B., Gautam, U.P., Koirala, B.P., Bhattarai, M., Kandel, T., Gupta, R.M., Timsina, C., Maharjan, N., Maharjan, K., Dahal, T., Hoste-Colomer, R., Cano, Y., Dandine, M., Guilhem, A., Merrer, S., Roudil, P., & Bollinger, L. (2015). The aftershock sequence of the 2015 April 25 Gorkha-Nepal earthquake. *Geophysical Journal International*, *203*(3), 2119–2124. https://doi.org/10.1093/gji/ggv412.

Aggarwal, S.K., Pastén, D., & Khan, P.K. (2017). Multifractal analysis of 2001 Mw7.7 Bhuj earthquake sequence in Gujarat, Western India. *Physica A: Statistical Mechanics and its Applications*, *488*, 177–186. https://doi.org/10.1016/j.physa.2017.06.022.

Aki, K. (1965). Maximum likelihood estimate of *b* in the formula Log *N*= *a* – *bM* and its confidence limits. *Bulletin of the Earthquake Research Institute, 43*, 237–239.

Avouac, J.P., Meng, L., Wei, S., Wang, T., & Ampuero, J.P. (2015). Lower edge of locked Main Himalayan Thrust unzipped by the 2015 Gorkha earthquake. *Nature Geoscience*, 8(9), 708–711. https://doi.org/10.1038/ngeo2518.

Bayrak, Y., & Bayrak, E. (2012). Regional variations and correlations of Gutenberg-Richter parameters and fractal dimension for the different seismogenic zones in Western Anatolia. Journal of Asian Earth Sciences, 58, 98–107. https://doi.org/10.1016/j.jseaes.2012.06.018.

Bayrak, Y., Yadav, R.B.S., Kalafat, D., Tsapanos, T.M., Çinar, H., Singh, A.P., Bayrak, E., Yilmaz, Ş., Öcal, F., & Koravos, G. (2013). Seismogenesis and earthquake triggering during the Van (Turkey) 2011 seismic sequence. *Tectonophysics, 601*, 163–176. https://doi.org/10.1016/j.tecto.2013.05.008.

Bilham, R. (2019). Himalayan earthquakes: A review of historical seismicity and early 21st century slip potential. *Geological Society Special Publication, 483*(1), 423–482. https://doi.org/10.1144/SP483.16.

Das, R., Wason, H.R., & Sharma, M.L. (2011). Global regression relations for conversion of surface wave and body wave magnitudes to moment magnitude. *Natural Hazards, 59*(2), 801–810. https://doi.org/10.1007/s11069-011-9796-6.

Falconer, K. (1997). Fractal Geometry. Biometrics, 53(3), 1183. https://doi.org/10.2307/2533585

Galetzka, J., Melgar, D., Genrich, J.F., Geng, J., Owen, S., Lindsey, E.O., Xu, X., Bock, Y., Avouac, J.-P., Adhikari, L.B., Upreti, B.N., Pratt-Sitaula, B., Bhattarai, T.N., Sitaula, B.P., Moore, A., Hudnut, K.W., Szeliga, W., Normandeau, J., Fend, M., Flouzalt, M. Bollinger, L., Shrestha, P., Koirala, B., Gautam, U., Bhattarai, M., Gupta, R., Kandel, T., Timsina, C., Sapkota, S.N., Rajaure, S., & Maharjan, N. (2015). Slip pulse and resonance of Kathmandu basin during the 2015 Mw 7.8 Gorkha earthquake, Nepal imaged with space geodesy. Science, 349(6252), 1091–1095. https://doi.org/10.1126/science.aac6383.

Gardner, J.K., & Knopoff, L. (1974). Is The Sequence of Earthquakes in Southern California, With Aftershocks Removed, Poissonian? *Bulletin of the Seismological Society of America, 64*(5), 1363–1367.

Ghazoui, Z., Bertrand, S., Vanneste, K., Yokoyama, Y., Nomade, J., Gajurel, A.P., & van der Beek, P.A. (2019). Potentially large post-1505 AD earthquakes in western Nepal revealed by a lake sediment record. *Nature Communications, 10*(1), 1–9. https://doi.org/10.1038/s41467-019-10093-4.

Ghosh, U. (2020). Seismic Characteristics and Seismic Hazard Assessment: Source Region of the 2015 Nepal Earthquake Mw 7.8 in Central Himalaya. *Pure and Applied Geophysics, 177*(1), 181–194. https://doi.org/10.1007/s00024-019-02318-w.

Gospodinov, D., Marekova, E., & Marinov, A. (2010). Verifying the dependence of fractal coefficients on different spatial distributions. *AIP Conference Proceedings, 1203*, 731–736. https://doi.org/10.1063/1.3322545.

Grassberger, P., & Procaccia, I. (1983). Characterization of

strange attractors. *Physical Review Letters, 50*(5), 346–349. https://doi.org/10.1103/PhysRevLett.50.346.

Gutenberg, B., & Richter, C.F. (1944). Frequency of earthquakes in California. *Bulletin of the Seismological Society of America*, 34, 185–188.

Hayes, G.P., Briggs, R.W., Barnhart, W.D., Yeck, W.L., McNamara, D.E., Wald, D.J., Nealy, J.L., Benz, H.M., Gold, R.D., Jaiswal, K.S., Marano, K., Earle, P.S., Hearne, M.G., Smoczyk, G.M., Wald, L.A., & Samsonov, S.V. (2015). Rapid characterization of the 2015 Mw 7.8 Gorkha, Nepal, earthquake sequence and its seismotectonic context. *Seismological Research Letters, 86*(6), 1557–1567. https://doi.org/10.1785/0220150145.

Helmstetter, A., Kagan, Y.Y., & Jackson, D.D. (2005). Importance of small earthquakes for stress transfers and earthquake triggering. *Journal of Geophysical Research: Solid Earth, 110*(5), 1–13. https://doi.org/10.1029/2004JB003286.

Hubbard, J., Almeida, R., Foster, A., Sapkota, S.N., Bürgi, P., Tapponnier, P., Wang, K., & Fialko, Y. (2015). Source characteristics of the 2015 Mw 7.8 Gorkha earthquake and its MW 7.2 aftershock from space geodesy. *Geology, 44*, 639–642. https://doi.org/10.1002/2015GL065201.

Kawamura, M., & Chen, K.H. (2017). Influences on the location of repeating earthquakes determined from a and b value imaging. *Geophysical Research Letters, 44*(13), 6675–6682. https://doi.org/10.1002/2017GL073335.

Khan, P.K., Ghosh, M., Chakraborty, P.P., & Mukherjee, D. (2011). Seismic b-value and the assessment of ambient stress in Northeast India. *Pure and Applied Geophysics, 168*(10), 1693–1706. https://doi.org/10.1007/s00024-010-0194-x.

Khattri, K.M., & Tyagi, A.K. (1983). Seismicity patterns in the Himalayan plate boundary and identification of the areas of high seismic potential. *Tectonophysics, 96*(3–4), 281–297. https://doi.org/10.1016/0040-1951(83)90222-6.

Letort, J., Bollinger, L., Lyon-Caen, H., Guilhem, A., Cano, Y., Baillard, C., & Adhikari, L.B. (2016). Teleseismic depth estimation of the 2015 Gorkha-Nepal aftershocks. *Geophysical Journal International, 207*(3), 1584–1595. https://doi.org/10.1093/gji/ggw364.

Lindsey, E.O., Natsuaki, R., Xu, X., Shimada, M., Hashimoto, M., Melgar, D., & Sandwell, D.T. (2015). Line-of-sight displacement from ALOS-2 interferometry: Mw 7.8 Gorkha Earthquake and Mw 7.3 aftershock. *Geophysical Research Letters, 42*(16), 6655–6661. https://doi.org/10.1002/2015GL065385.

Lopes, R., & Betrouni, N. (2009). Fractal and multifractal analysis: A review. *Medical Image Analysis, 13*(4), 634–649. https://doi.org/10.1016/j.media.2009.05.003.

Mandal, P., & Rodkin, M.V. (2011). Seismic imaging of the 2001 Bhuj Mw 7.7 earthquake source zone: B-value, fractal dimension and seismic velocity tomography studies. *Tectonophysics, 512*(1–4), 1–11. https://doi.org/10.1016/j.tecto.2011.09.004.

Mogi, K. (1967). Earthquakes and fractures. *Tectonophysics, 5*(1), 35–55. https://doi.org/10.1016/0040-1951(67)90043-1.

Mugnier, J.L., Jouanne, F., Bhattarai, R., Cortes-Aranda, J., Gajurel, A., Leturmy, P., Robert, X., Upreti, B., & Vassallo, R. (2017). Segmentation of the Himalayan megathrust around the Gorkha earthquake (25 April 2015) in Nepal. *Journal of Asian Earth Sciences, 141*, 236–252. https://doi.org/10.1016/j.jseaes.2017.01.015.

Naimi-Ghassabian, N., Khatib, M.M., Nazari, H., & Heyhat, M.R. (2018). Regional variations and earthquake frequency–magnitude distribution and fractal dimension in the North of Central-East Iran Blocks (NCEIB). *Arabian Journal of Geosciences, 11*(11), 243–264. https://doi.org/10.1007/s12517-018-3506-6.

Nampally, S., Padhy, S., & Dimri, V.P. (2018). Characterizing spatial heterogeneity based on the b-value and fractal analyses of the 2015 Nepal earthquake sequence. *Tectonophysics, 722*, 154–162. https://doi.org/10.1016/j.tecto.2017.11.004.

Oncel, A.O., & Wilson, T. (2007). Anomalous seismicity preceding the 1999 Izmit event, NW Turkey. *Geophysical Journal International, 169*(1), 259–270. https://doi.org/10.1111/j.1365-246X.2006.03298.x.

Oncel, A.O., & Wilson, T.H. (2002). Space-time correlations of seismotectonic parameters: Examples from Japan and from Turkey preceding the İzmit earthquake. *Bulletin of the Seismological Society of America, 92*(1), 339–349. https://doi.org/10.1785/0120000844.

Pailoplee, S., & Choowong, M. (2014). Earthquake frequency-magnitude distribution and fractal dimension in mainland Southeast Asia. *Earth, Planets and Space, 66*(1), 1–10. https://doi.org/10.1186/1880-5981-66-8.

Radziminovich, N.A., Miroshnichenko, A.I., & Zuev, F.L. (2019). Magnitude of completeness, b-value, and spatial correlation dimension of earthquakes in the South Baikal Basin, Baikal Rift System. *Tectonophysics, 759*, 44–57. https://doi.org/10.1016/j.tecto.2019.04.002.

Rodríguez Pascua, M.A., De Vicente, G., Calvo, J.P., & Perez-Lopez, R. (2003). Similarities between recent seismic activity and paleoseismites during the late miocene in the external Betic Chain (Spain): Relationship by "b" value and the fractal dimension. *Journal of Structural Geology, 25*(5), 749–763. https://doi.org/10.1016/S0191-8141(02)00078-0.

Roy, P.N.S., & Padhi, A. (2007). Multifractal analysis of earthquakes in the Southeastern Iran-Bam Region. *Pure and Applied Geophysics, 164*(11), 2271–2290. https://doi.org/10.1007/s00024-007-0272-x

Roy, P.N.S., & Ram, A. (2006). A correlation integral approach to the study of 26 January 2001 Bhuj earthquake, Gujarat, India. *Journal of Geodynamics, 41*(4), 385–399. https://doi.org/10.1016/j.jog.2005.10.003.

Scholz, C.H. (1968). The frequency-magnitude relation of microfracturing in rock and its relation to earthquakes. Bulletin of the Seismological Society of America, 58(1),

399–415. https://doi.org/10.1785/bssa0580010399

Scholz, C.H., & Campos, J. (2012). The seismic coupling of subduction zones revisited. *Journal of Geophysical Research: Solid Earth, 117*(5), 1–22. https://doi.org/10.1029/2011JB009003.

Schorlemmer, D., Wiemer, S., & Wyss, M. (2005). Variations in earthquake-size distribution across different stress regimes. *Nature, 437*(7058), 539–542. https://doi.org/10.1038/nature04094.

Shi, Y., & Bolt, A.B. (1982). The standard error of the magnitude-frequency b value. *Bulletin of the Seismological Society of America*, 72(5), 1677–1687.

Singh, C., Singh, A., & Chadha, R.K. (2009). Fractal and b-value mapping in eastern Himalaya and southern Tibet. *Bulletin of the Seismological Society of America, 99*(6), 3529–3533. https://doi.org/10.1785/0120090041.

Sobiesiak, M., Meyer, U., Schmidt, S., Götze, H.J., & Krawczyk, C.M. (2007). Asperity generating upper crustal sources revealed by b value and isostatic residual anomaly grids in the area of Antofagasta, Chile. *Journal of Geophysical Research: Solid Earth, 112*(12). https://doi.org/10.1029/2006JB004796.

Sreejith, K.M., Sunil, P.S., Agrawal, R., Saji, A.P., Rajawat, A.S., & Ramesh, D.S. (2018). Audit of stored strain energy and extent of future earthquake rupture in central Himalaya. *Scientific Reports, 8*(1), 1–9. https://doi.org/10.1038/s41598-018-35025-y.

Tiwari, R.K., & Paudyal, H. (2021). Variability of b-value before and after the Gorkha earthquake in the central Himalaya and vicinity. *Bibechana, 18*(2), 32–42. https://doi.org/10.3126/bibechana.v18i2.31207.

Tosi, P. (1998). Seismogenic structure behaviour revealed by spatial clustering of seismicity in the Umbria-Marche Region (Central Italy). *Annali Di Geofisica, 41*(2), 215–224. https://doi.org/10.4401/ag-4331.

Wiemer, S. (2001). A software package to analyze seismicity: ZMAP. *Seismological Research Letters, 72*(3), 373–382. https://doi.org/10.1785/gssrl.72.3.373.

Wiemer, S., & Wyss, M. (2000). Minimum magnitude of completeness in earthquake catalogs: Examples from Alaska, the Western United States, and Japan. *Bulletin of the Seismological Society of America, 90*(4), 859–869. https://doi.org/10.1785/0119990114.

Wyss, M. (1973). Towards a Physical Understanding of the Earthquake Frequency Distribution. *Geophysical Journal of the Royal Astronomical Society, 31*(4), 341–359. https://doi.org/10.1111/j.1365-246X.1973.tb06506.x.

Yin, L., Li, X., Zheng, W., Yin, Z., Song, L., Ge, L., & Zeng, Q. (2019). Fractal dimension analysis for seismicity spatial and temporal distribution in the circum-Pacific seismic belt. *Journal of Earth System Science, 128*(1), 1–7. https://doi.org/10.1007/s12040-018-1040-2.

Yue, H., Simons, M., Duputel, Z., Jiang, J., Fielding, E., Liang, C., Owen, S., Moore, A., Riel, B., Ampuero, J.P., & Samsonov, S.V. (2017). Depth varying rupture properties during the 2015 Mw 7.8 Gorkha (Nepal) earthquake. *Tectonophysics, 714–715*, 44–54. https://doi.org/10.1016/j.tecto.2016.07.005.

Zamani, A., & Agh-Atabai, M. (2011). Multifractal analysis of the spatial distribution of earthquake epicenters in the Zagros and Alborz-Kopeh Dagh regions of Iran. *Iranian Journal of Science and Technology, Transaction A: Science, 35*(1), 39–51. https://doi.org/10.22099/ijsts.2011.2127.